



Development of a High Throughput Sample Holder for Crystallography

Christina Müller, TU Kaiserslautern, Germany

Supervisors: Dennis Dierksmeyer, Dr. Dennis Göries, Dr. Alke Meents

September 9, 2015

Abstract

The following report presents the development of the supporting material of a high throughput sample holder for crystallography experiments at synchrotron facilities such as the P11 beamline at PERTA III. In this setup microcrystals are aligned in small holes in a polyimide-tape that is driven through the X-ray beam ensuring a rapid replacement of the destroyed sample. To achieve the required hole size of few micrometers and a well defined hole distance two lasers of different wavelength (UV and NIR range) and pulse duration are applied and the results are compared to find the best solution for the process.

Contents

1	Introduction and Objective	2
2	Theory and Materials	3
2.1	Overall design of the sample holder	3
2.2	Supporting material	4
2.3	Experimental setup	4
2.4	Impact of UV- and IR-lasers on polyimide	7
2.5	Impact of short pulsed IR-lasers on Diamond	8
3	Conduct and Results	8
3.1	Resolution of the on-axis CCD camera	8
3.2	Generation of holes in polyimide with the Nd:YAG laser	8
3.3	Generation of holes in polyimide with the ultrashort pulsed Pharos laser	11
3.4	Micromachining of diamond with the ultrashort pulsed Pharos laser	13
4	Conclusion	17
5	References	18
6	Pictorial Sources	20

1 Introduction and Objective

First discovered as an undesired energy loss in particle accelerators, synchrotron radiation became one of the most important tools in numerous application areas such as material science, medicine, biology and chemistry. As a source of electromagnetic waves of high brilliance and a huge spectral range of selectable wavelengths from infrared (700 nm - 1 mm) to X-ray (0.01 nm -10 nm) it is among others utilized for structure determinations of biological systems in crystallography. Therefore new third generations accelerators such as PETRA III at DESY are designed to create synchrotron radiation using periodic magnet arrays, so-called undulators. After injection into the storage ring the particles (electrons or positrons) are accelerated close to the speed of light and pass the ring in small bunches. Each time they pass bending magnets, they emit electromagnetic waves due to transverse acceleration, the so-called bremsstrahlung. Undulators force the particle on a curved trajectory thus leading to a reinforcement of radiation. A combination of relativistic effects, the Doppler-effect and the properties of the magnetic field results in an X-ray beam of high photon flux per time, energy, solid angle and source area [1]. For the resolution of structures in the range of angstroms as in protein crystallography, X-rays are crucial since the resolution d is limited by the applied wavelength [2] according to the bragg equation

$$n * \lambda = 2 * d * \sin \theta \quad (1)$$

In this method electromagnetic waves are scattered on the electrons of the regularly orientated proteins in the crystal. The resulting diffraction pattern contains the information about the electron density which has to be analysed to deduce the protein structure. Traditional X-ray crystallography is based on irradiation of large crystals of sizes up to several hundred micrometers under different irradiation angles. Preparation and mounting of the samples require a significant amount of time and are difficult to perform [3]. Focusing the radiation on areas of a few square micrometers allows structure determinations from microcrystals or even single molecules. However radiation damage via the photoelectric effect or compton-scattering limits the crystal lifetime to few seconds at synchrotron-sources [3], [4].

A first demand on sample holders is thus a high-throughput setup to achieve a fast replacement of the destroyed microcrystals with a possible synchronisation to X-ray flashes as in the future XFEL. A second aspect is to reduce its contribution to background scattering, since the bragg intensities of the microcrystals are otherwise difficult to distinguish from the background [3]. The objective of this work is to contribute in the development of a high throughput sample holder for microcrystals that are analysed at the P11 beamline at PETRA III.

2 Theory and Materials

2.1 Overall design of the sample holder

The setup of the high throughput sample holder is similar to a tape deck where two wheels let the medium (here a polyimide-tape supporting the microcrystals) pass the measurement device (here the X-ray beam). In the following figure 1 the design of the high throughput sample holder is presented:

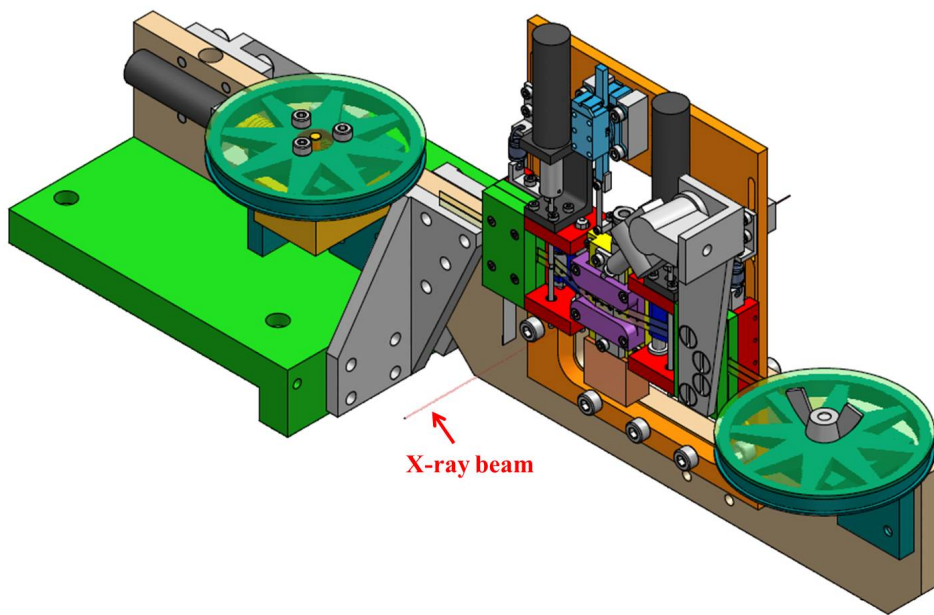


Figure 1: Design of the high throughput sample holder with the polyimide-tape as supporting material [1].

For the X-ray beam (red line) comes in sideways, the tape has to be aligned perpendicular to the ray to avoid a grazing incidence angle and associated scattering effects of the substrate. Small holes in the polyimide-tape carry the microcrystals that are pipetted on the substrate in their mother liquid via a glass-capillary shortly before the measurement takes place. A robotic arm (grey) can be used to position of the capillary in all three spatial directions. A suction device removes the liquor, so microcrystals larger than the hole-diameter are retained. The polyimide-tape is directed and kept tense via a system of rolls (blue). Two rotating motors (black) drive the rolls and precisely define the tape velocity. A third motor controls one of the wheels to keep a certain tape tension. The tape is further stabilized with a duct (purple) at the place where the beam impinges on the sample. The precision tuning of this duct takes place via a piezo motor (light blue) to match the centre of the tape holes to the beam-position.

2.2 Supporting material

In X-ray experiments polyimide and beryllium are the most commonly used materials for windows as they show a high transmittance in this spectral range [5]. Polyimide is highly stable over a wide temperature range from 15 K up to more than 500 K. This is crucial for the application as a sample holder for both high and very low temperatures can occur [6]. Previous measurements indicate that polyimide shows a lower and less structured background scattering compared to beryllium [5]. As polyimide is non-toxic and a low-cost material it is both easy to handle and replaceable during the operation of the sample holder [6]. With these properties it is a convenient support material for the microcrystals. The here used polyimide-tape is provided by the company *Capling* with a thickness of 12.5 μm and a width of 6.4 mm [7].

2.3 Experimental setup

The main issue of the presented experiments is to find a possibility to produce holes in the polyimide-tape with a diameter about 5 μm in a well-defined distance to each other. In former research concerning sample holders for microcrystals it was found that micropores of 2 - 5 μm of different geometry are suitable to avoid a preferred orientation of the crystals which would lead to incomplete datasets of the X-ray intensity [3].

As they are widely utilized for material machining, a Nd:YAG Laser (*Elforlight SPOT laser systems*) is used in the first attempt to create holes in the support material. This laser emits 1.5 ns-pulses of the fundamental wavelength 1064 nm and higher harmonics (532 nm and 355 nm) due to frequency doubling and tripling via a nonlinear optical medium [8]. In this setup two mirrors reflecting in UV-range were used to select the 355 nm part. Further mirrors and a Schwarzschild-objective (*Newport, 15x*, working distance 24 mm) were used to direct and focus the laser on a piece of polyimide-tape that was fixed in a clamping device. This device was mounted on linear stages that were controlled by a python script so the tape could be moved relative to the laser beam in different two-dimensional patterns. A computer-driven mechanical Shutter ensured a defined illumination duration of the sample. The Schwarzschild-optic for microscopes consists of a concave primary mirror facing the sample and a secondary convex mirror. Properties as zero chromatic aberration and neglectable spherical aberration, astigmatism or coma over a wide spectral range from 200 nm to 20 μm allow for a good focusing of the here used laser [9]. The insertion of an inverted Galilean telescope in the beam path leads to a widening of the laser-beam resulting in a smaller focal spot according to the relation of beam divergence θ_{div} and beam waist ω_0 that describes a Gaussian beam profile [10].

$$\theta_{\text{div}} = \arctan \left(\frac{\lambda}{\pi * \omega_0} \right) \quad (2)$$

Two CaF_2 lenses, one biconvex (focal distance $f_1 = -30 \text{ mm}$) and one biconcave lens (focal distance $f_2 = 100 \text{ mm}$) lead to a widening of the beam-radius by a factor of $F = -f_1/f_2 = 3,33$ [11]. Figure 2 shows the experimental setup with the Nd:YAG laser:

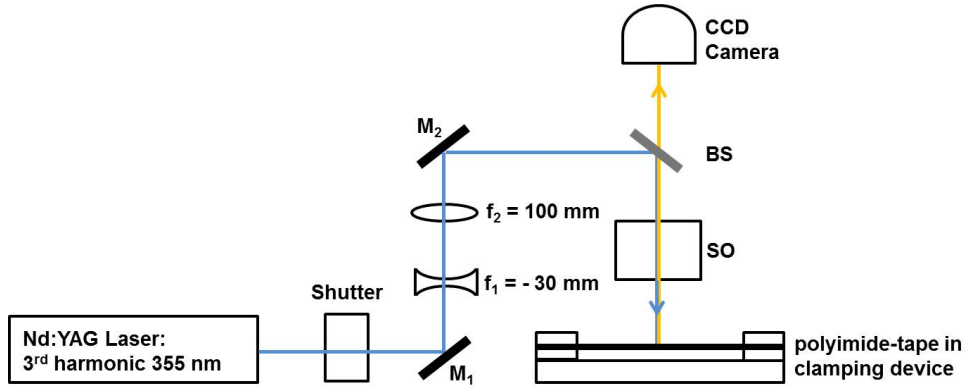


Figure 2: Beam path with UV-mirrors (M_1 and M_2), the "hot mirror" working as a beam splitter (BS), the focusing Schwarzschild-objective (SO) and the two inserted CaF_2 lenses (f_1 and f_2) to widen the laser beam.

In a second attempt to create holes in the polyimide-tape, a Yb:KGW (ytterbium doped potassium gadolinium tungstate) laser system (*Light Conversion, Pharos*) emitting fs-pulses of 1030 nm wavelength was utilized. It is based on chirped-pulse amplification where a dispersive stretcher chirps and temporally broadens the pulse resulting in a reduced peak power. This allows the pulse to undergo further amplification in the gain medium without destroying it. A compressor with the opposite dispersion temporally compresses the pulse removing the chirp and emits a pulse with enhanced intensity [12]. Changing the compressor length allows for a tunable output pulse duration from 160 fs to 10 ps [13]. The laser beam was directed on the sample via protected silver mirrors and then focused by a "High Power MicroSpot Focusing Objective" (*Thorlabs LMH-5x-1064 resp. LMH-20x-1064*, working distance 40 mm resp. 10 mm). The following outline (figure 3) shows the beam path for the Pharos-laser:

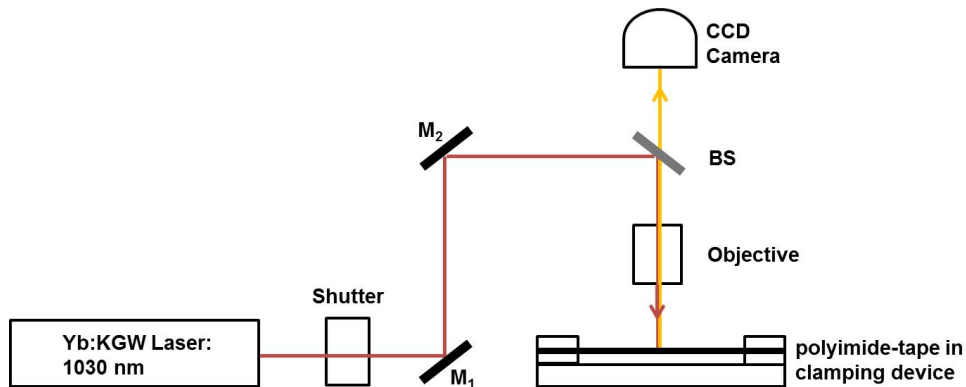


Figure 3: Beam path with protected silver mirrors (M_1 and M_2), the beam splitter (BS) and the focusing Objective.

The impact of the laser light on the tape was directly visualized by an on-axis CCD-camera (*Prosilica GC*) as shown in figure 4. A "hot mirror" for the Nd:YAG laser and a fiber laser mirror for the Pharos-laser reflects ca. 85 % of the incoming 355 nm [14] or ca. 99.5 % of the 1030 nm [15] on the sample and transmits the backscattered VIS-part of the light.

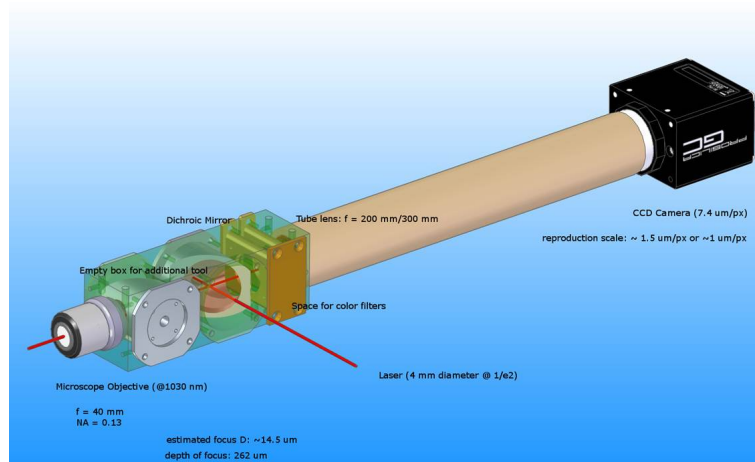


Figure 4: Scheme of the on-axis CCD-camera with a beam splitter cavity [2].

2.4 Impact of UV- and IR-lasers on polyimide

The following figure 5 shows the chemical structure of polyimide:

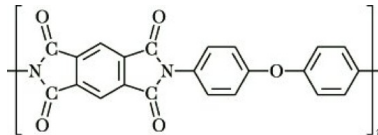


Figure 5: Chemical structure of Polyimide [3].

Absorption spectra display that polyimide shows strong absorption in the UV-range. Thus most efficient laser ablation takes place when a laser with a wavelength about 300 nm is used [16]. In former research different processes leading to material degradation of Polyimide are discussed. Studies of the influence of a ns pulsed 351 nm laser on Polyimide assume bond dissociation energies in a range from 5 to 8 eV. For that reason photochemical bond-breaking due to single-photon absorption at this wavelength was rated unlikely but the contribution of photopyrolysis was estimated more probably. In this mechanism vibrational excitation of the molecules leads to a local heating of the material. For Polyimide shows a rather low thermal diffusivity ($k \sim 10^{-3} \text{ cm}^2/\text{s}$) this heating is concentrated in a small light absorption depth which causes bond breaking and ejection of small fragments resulting in local ablation of the material [16]. Other research groups assume binding energies from 3 to 3,5 eV as they are found for covalent bonds as C-C, C-N and C-O which appear in Polyimide. However, analyses of single-shot experiments revealed an activation energy about 1 eV. This was explained via a photophysical model where the molecule is electronically excited, so less energy is needed for the degradation. However this is supposed to be more relevant for ps pulses that are in the same order as the thermal relaxation time $t_s = 36 \text{ ps}$. Thermal effects were presumed to be the main factor to ablation for ns pulses. In this case volatile species as CO are removed from the bulk material. The assumption that the loss of two carbonyl groups in the same imide ring could result in the cut of the polymer chains and thus lead to the ablation of the remaining material can be supported by other investigations [17]: IR spectral analyses of vapours that emerged during the experiment indicate that they indeed consist of light fragments such as CO [16], [18].

Other sources report on several absorption bands in the MIR ($5 \mu\text{m} - 50 \mu\text{m}$) leading to thermal ablation of the material. Experiments with wavelengths of $9 \mu\text{m}$ and $10.6 \mu\text{m}$ revealed that the smaller wavelength resulted in well-defined edges-regions of the holes. Application of lasers in the NIR-region are thought to produce charring of the irradiated area for Polyimide shows only weak absorbance in this range [19]. To examine the impact of NIR-irradiation, the Pharos laser was utilised.

2.5 Impact of short pulsed IR-lasers on Diamond

Another material that is employed for X-ray windows at synchrotron facilities is diamond for it combines properties like extreme hardness and chemical inertness with high transparency for X-rays. Treatment of this material with industrial lasers in the NIR range is possible via multiphoton absorption demanding a short-pulsed laser source [20]. A further aim of this project is to use the Pharos-laser for drilling holes smaller than 1 mm diameter in diamond.

3 Conduct and Results

3.1 Resolution of the on-axis CCD camera

To determine the resolution of the CCD camera, a US Air Force test chart was utilized. It consists of a pattern of bars that are divided into group numbers and elements. The resolution limit of the tested optic is reached when two bars cannot be distinguished. The following figure 6 shows a picture of the smallest pattern on the target recorded by the camera.



Figure 6: Recorded picture of the smallest USAF test chart pattern.

The achieved resolution can be identified via tabulations [21]. In this case element 6 of group 7 corresponds to a resolution of $2.19 \mu\text{m}$. However it must be taken into account that systematical errors as vibrations of the table and motions in the surrounding area lead to a degradation of the theoretical resolution during the measurement.

3.2 Generation of holes in polyimide with the Nd:YAG laser

After a coarse adjustment of the optical elements of the beam path the laser-focus on the test piece of polyimide had to be adjusted to the optical axis of the camera.

To localize the focus in the sector the camera showed, a small Ce:YAG crystal plate that was put on top of the polyimide-tape. Excitation with a wavelength about 350 nm leads to strong emission in the range of 500 to 600 nm that helps to find the focus and further improve its quality [22]. A photodiode was utilised to measure the average power of the laser before the position of the shutter. For the generation of holes linear stages and shutter were controlled by the computer via different python-scripts that defined the x- and y-position of the tape and the exposure time (see attachment). The results were examined with an inverse light microscope (*Nikon Eclipse Ti*) using a 10-fold magnification for overviews and a 40-fold magnification for measurements of the hole-diameter. The following figure 7 shows the first result of holes that were produced with the Nd:YAG laser without beam-expansion.

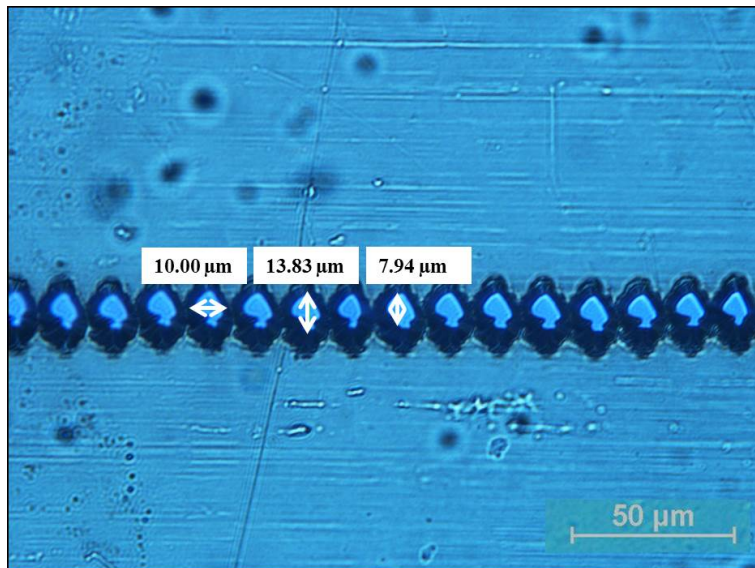


Figure 7: 40-fold magnification of holes in the polyimide-tape without expansion of the Nd:YAG laser beam.

It can be observed that all produced holes are surrounded by an edge that appears dark and could descend from a crater-like formation of the holes. In former research there is evidence for the formation of humps and dents during UV-laser irradiation that supports this theory [18]. It is also possible that the changed transmission-properties in the edge region results from incompletely combusted organic material. This is reported to lead to a brownish looking substance near the edge of the formed holes [16]. In addition to that all holes show a strong deformation of the edge that could be explained by a bad beam-quality due to marginal misalignment of the laser itself or problems with the subsequent optical components. The first attempt to create holes was conducted with a beam splitter that was former used in an X-ray-experiment and therefore equipped with a

small hole in the centre to avoid destruction. This lead to perturbations during the alignment and is thought to contribute to the bad beam-quality. With a size about $14\text{ }\mu\text{m} \times 10\text{ }\mu\text{m}$ the desired diameter is not reached yet. For that reason the focus had to be reduced inserting the inverted Galilean telescope into the beam path. Also the pierced beam splitter was replaced by the "hot mirror". The following figure 8 shows an overview of different possible hole patterns and the measurement of holes after the assembly of the additional and new components.

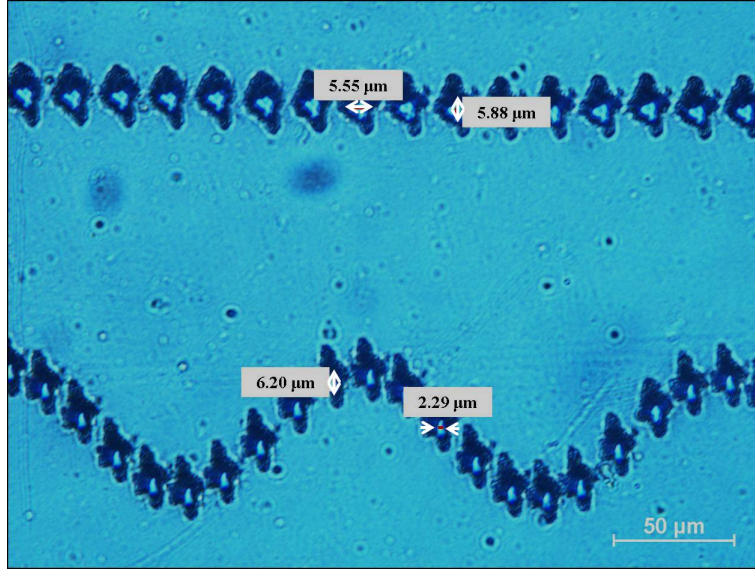


Figure 8: Different hole patterns with 40-fold magnification with former expansion of the Nd:YAG laser beam.

Still the holes show a dark, irregular border indicating a bad beam quality. However a direct comparison of the pictures before and after the insertion of the "hot mirror" shows that it slightly contributes to an improvement of the focus for the border-line of the holes then appears more regular. This supports the assumption that the beam-quality is mainly diminished by a misalignment of the laser. The inverted Galilean telescope achieved the expected reduction of the hole diameter to an adequate size of $5.6\text{ }\mu\text{m} \times 5.9\text{ }\mu\text{m}$ which roughly accords with theory. The results were achieved with a repetition rate f_R of 12.3 kHz ($\pm 1\text{ kHz}$) and an average power P_{av} of 42 mW ($\pm 2\text{ mW}$). According to the Definition $P_{av} = W * f_R$, a pulse energy of $3.4\text{ }\mu\text{J}$ ($\pm 0.4\text{ }\mu\text{J}$) was reached, which further sustains the suspicion about a problem with the laser for the datasheet indicates a possible pulse energy of $10\text{ }\mu\text{J}$ for 355 nm . However with the measured focus-diameter of approximately $5.8\text{ }\mu\text{m}$ ($\pm 0.2\text{ }\mu\text{m}$), an energy density of $13.1\text{ J/cm}^2 \pm 3\text{ J/cm}^2$ was sufficient to create holes in the material. A comparison of the holes in line and the holes in the sinus-pattern reveals a difference in scale and form which could relate to the exposure time that was shorter for the sinus-pattern. The

impact of exposure time on the hole-quality was examined for some holes in line as represented in the following figure 9 for 1 s and 0.2 s:

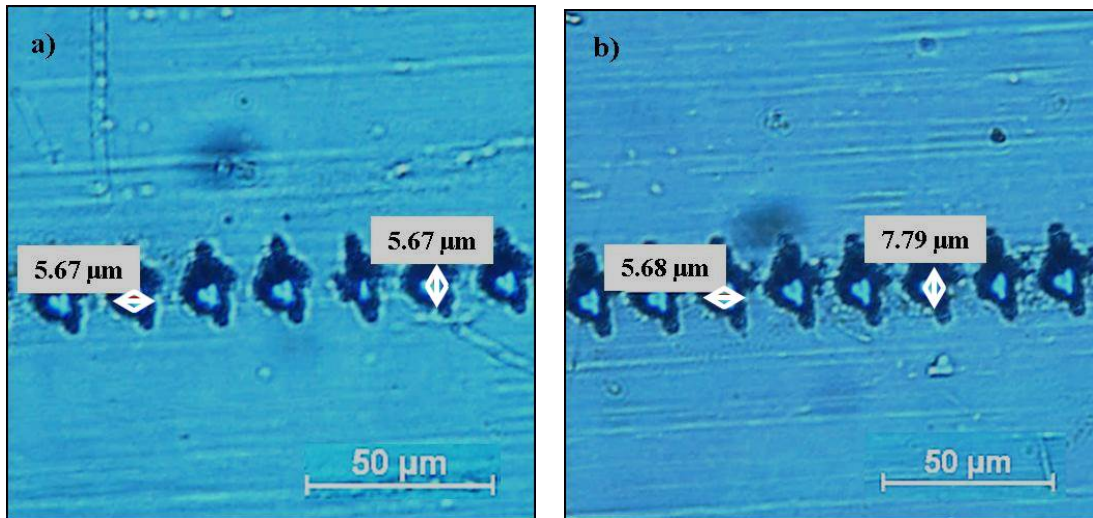


Figure 9: Impact of different exposure time on the hole diameter conducted with the Nd:YAG laser. a) 0.2 s b) 1 s

A direct comparison of the pictures indicates that shorter exposure times lead to smaller holes. This impact is most prominent in the vertical direction where an irradiation for 1 s results in $7.8 \mu\text{m}$ whereas an exposure time of 0.2 s leads to $5.7 \mu\text{m}$ holes. The impact of exposure time in the horizontal direction is neglectable as the difference is in the region of measurement accuracy. This could be explained by the above mentioned misalignment of the laser which results in a focus that strongly differs from a TEM 00 mode.

3.3 Generation of holes in polyimide with the ultrashort pulsed Pharos laser

After the adjustment of the optical elements of the beam path a photodiode was utilised to measure the average power of the laser. As in the former experiments with the Nd:YAG laser the sample was mounted on linear stages to determine its position via python scripts that also controlled the integrated shutter system of the Pharos laser to assure a well defined exposure time. The first attempt to create holes in the tape was conducted with a high-power objective of 5-fold magnification. The following figure 10 shows the results for exposure times of 0.05 s and 0.2 s:

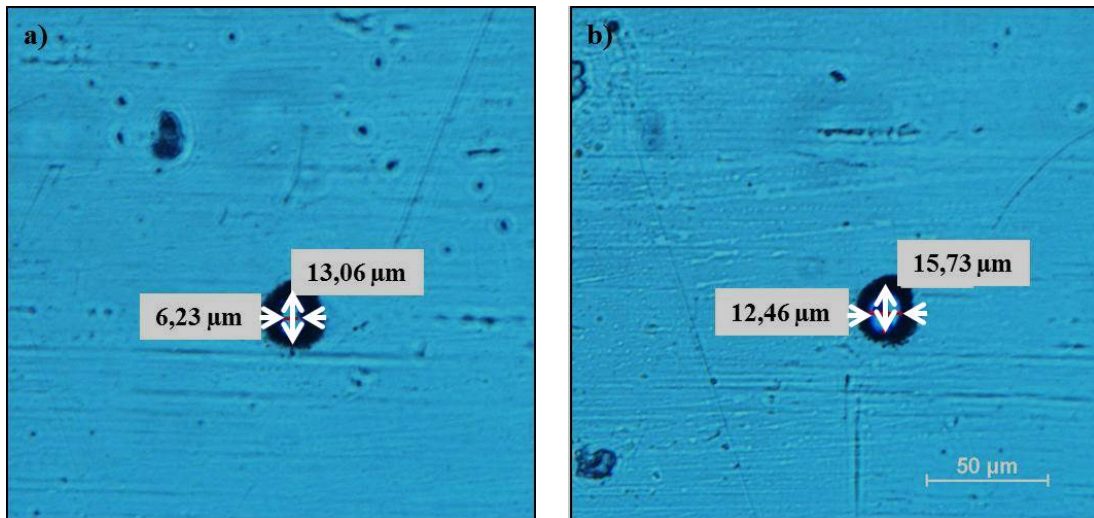


Figure 10: Impact of different exposure times on the hole diameter conducted with the Pharos laser a) 0.05 s b) 0.2 s

The hole diameter slightly decreases with a shorter exposure time. In this section all holes were produced with a repetition rate f_R of 5 kHz and an average power P_{av} of 52 mW (± 2 mW). A pulse energy of $10.4 \mu\text{J}$ ($\pm 0.4 \mu\text{J}$) for 0.05 s was thus sufficient to produce a hole that almost satisfies the required $5 \mu\text{m}$ diameter. Similar to the results of the Nd:YAG laser the holes are surrounded by a dark edge that could descend either from a sloped boundary or charring effects as mentioned in part 2.4 [19]. To further reduce the focal diameter an objective with 20-fold magnification leading to an increased beam divergence was applied. In figure 11 the results for an exposure time of 0.05 s and 0.1 s are presented:

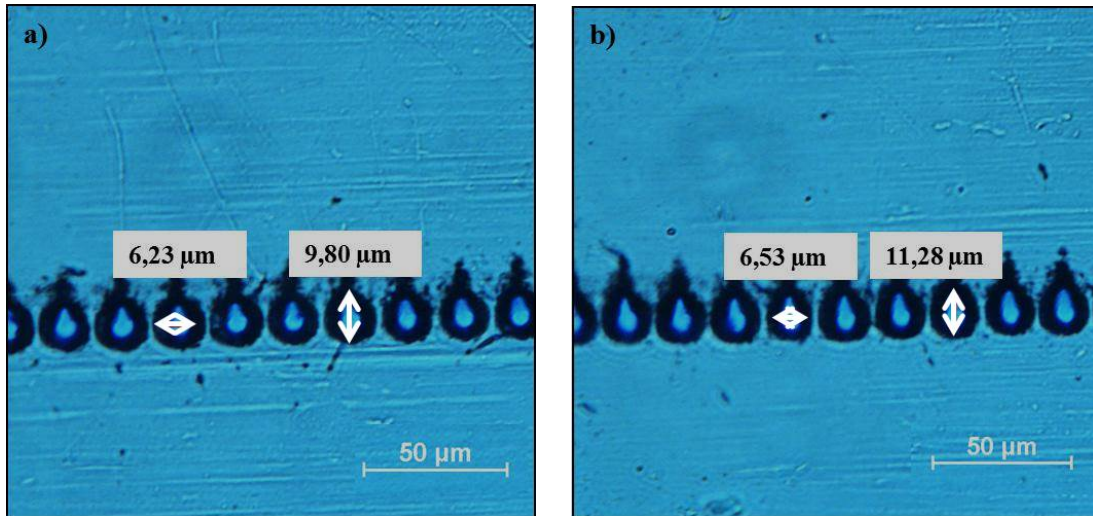


Figure 11: Impact of different exposure times on the hole diameter with the 20-fold magnification objective conducted with the Pharos laser a) 0.05 s b) 0.1 s

A direct comparison between the results achieved with the 5-fold and 20-fold objective after illumination for 0.05 s shows that the insertion of the new objective acquired a reduction of the focal spot in the vertical direction. For a higher exposure time of 0.1 s the value measured with the 20-fold objective is with 11.28 μm still smaller than the 13.06 μm that were obtained with the 5-fold magnification with an exposure time of 0.05 s which further suggests a successful reduction of the focal diameter. However the appearance of the hole changed to a less regular form. It is possible that the position of the tape did not match with the focal plane for the decrease of the axial resolving power impeded the alignment of the focus on the tape [23]. The distortion of the holes could also derive from polarisation effects for the Pharos laser emits linear polarised light [13]. This could result in a direction-dependant interaction of the radiation with the polyimide. To examine the effect of the polarisation on the result a quarter wave plate could be inserted into the beam path. A 45° turn of the optical axis of the plate relative to the direction of polarisation leads via double refraction to a $\pi/2$ phase shift of ordinary and extraordinary ray resulting in circular polarized light [24]. Hence no anisotropic ablation due to polarisation effects is to be expected.

3.4 Micromachining of diamond with the ultrashort pulsed Pharos laser

In the following preparatory experiments for laser machining of diamond are presented. A python script was used to create a circle of 1 mm diameter in

the polyimide-tape under permanent laser irradiation. To avoid a bulge at the beginning of the circle when the laser beam rests for a time at the start position and to remove the drilling core it is moved from the centre of the circle on a spiral trajectory to a circular path. The following figure 12 illustrates the procedure based on a 1 mm test hole with the Nd:YAG laser:

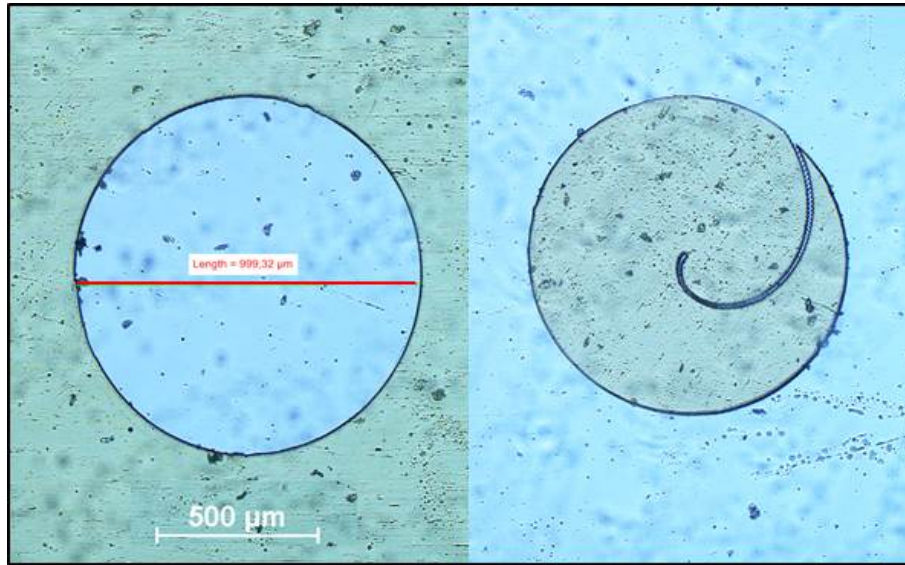


Figure 12: a) 1 mm diameter hole in polyimide-tape b) spiral trajectory on cut off polyimide peace performed with the Nd:YAG laser.

Further experiments were conducted with the Pharos laser. For this experiments the same setup that was utilized for the generation of holes in polyimide with the 5-fold magnification objective was used without a quarter wave plate. To achieve a blind hole in the diamond, ablation has to take place in small and well-defined steps with increasing drill depth. For that reason the ablation threshold at the focal spot had to be determined. In several preliminary tests it was found that a repetition rate f_R of 5 kHz and an average power P_{av} of 50 mW (± 2 mW) lead to substantial ablation in a broad area around the focal spot. Via a pulse picker divider, the amount of transmitted pulses from the entire pulse train can be reduced. In this way the repetition rate was reduced to 1 kHz for the micromachining experiments. The hole diameter was measured using the inverted microscope of the former experiments as presented in figure 13:

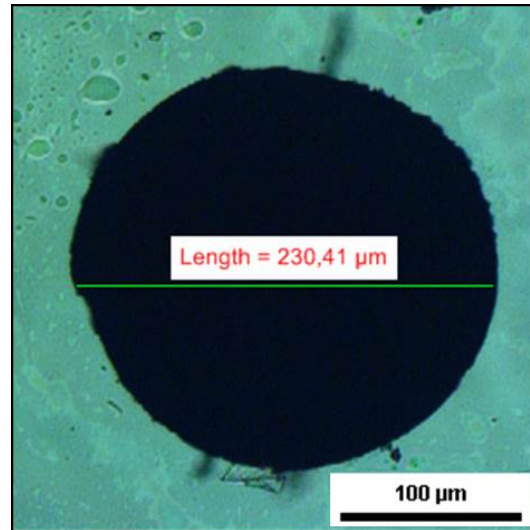


Figure 13: Laser drilled hole in diamond observed with 10-fold magnification of the inverted microscope.

Moving the diamond on a spiral trajectory through the laser beam lead to a complete ablation of the drilling core. Holes of diameters about $200\text{ }\mu\text{m}$ could successfully be produced with the applied laser settings and python scripts in a reasonable time. To examine the drilling depth an incident light microscope (*Carl Zeiss Axioscope*) with 20-fold magnification was utilised. The difference in height of the microscope table between focus on the diamond surface and the base of the blind hole was measured via a measuring sensor and amounted to $60\mu\text{m}$ ($\pm 2\text{ }\mu\text{m}$). A higher dwelling time in the centre resulted in a conical blind hole. Figure 14 presents pictures of three different focal planes on the diamond hole:



Figure 14: Pictures of different focal planes with the 20-fold magnification objective of the incident light microscope.

A further improvement of the hole quality was achieved by decreasing the laser power and accepting a longer duration of the experiment. More spiral passages

are necessary to remove the drilling core entirely. Using the 20-fold magnification objective and the quarter wave plate are expected to lead to a further refinement of the edge quality of the hole.

4 Conclusion

The objective to prepare the supporting material for the high throughput sample holder for crystallography experiments was reached. The required hole size to retain microcrystals from their mother liquor was achieved with the Nd:YAG laser. Micromachining of diamond was successfully realised using the ultrashort pulsed Pharos laser.

Treatment of the polyimide-tape with the Nd:YAG laser lead to holes with a diameter about 10 μm . The insertion of an inverted Galilean telescope achieved the expected effect of a beam expansion leading to higher beam divergence. This resulted in a smaller focus and thus holes smaller than 6 μm . It is assumed that due to an irregular hole shape the crystals may arrange in a variable orientating that could be convenient regarding the subsequent measurements as mentioned in chapter 2.3.

Contrary to the expectations, using the Pharos laser lead to thermal ablation of polyimide resulting in holes of defined measurements without intense charring effects. A further improvement of the focal spot reducing the hole diameter to almost the desired diameter was reached with the utilisation of a 20-fold magnifying objective. A future insertion of a quarter wave plate into the beam path should further reduce the hole diameter due to elimination of polarisation effects.

Micromachining of diamond with the Pharos laser via multiphoton ablation was successfully realised producing holes with diameters distinctly smaller than 500 μm . To improve the hole quality further investigations using the 20-fold magnification and the quarter wave plate are necessary. In a different approach for micromachining of diamond, lasers of different wavelengths could be applied in future research as diamond shows higher absorption in the UV or MIR range [25]. For wavelengths smaller than 225 nm single photon absorption leads to excitation of electrons from valence to conduction band [20]. Therefore it would be interesting to investigate photochemical bond-breaking applying UV lasers in addition to the here presented thermal ablation of the material.

5 References

- [1] G. Margaritondo. *Elements of Synchrotron Light for Biology, Chemistry and Medical Research*. Oxford University Press, 2002.
- [2] W. Demtröder. *Experimentalphysik III Atome, Moleküle und Festkörper*. Springer Verlag, 2005.
- [3] P. Roedig et al. A micro-patterned silicon chip as sample holder for macromolecular crystallography experiments with minimal background scattering. *Sci. Rep.*, 5, 2015.
- [4] R. Neutze et al. Potential for biomolecular imaging with femtosecond x-ray pulses. *Nature*, 406:752–757, 2000.
- [5] R. W. Alkire and F. J. Rotella. An incident-beam monitor for use in protein crystallography at a synchrotron source. *J. Appl. Cryst.*, 30:327–332, 1997.
- [6] M. Meserschmidt et al. Ultra-low-temperature x-ray data collection with a newly developed 0.1 mm kapton-film cylinder for a closed-cycle helium cryostat. *J. Appl. Cryst.*, 36:1452–1454, 2003.
- [7] Caplinq Corporation. <http://www.caplinq.com/0.5-mil-polyimide-kapton-film-no-adhesive-pit0.5n-series.html>.
[Online accessed 01-September-2015].
- [8] Elforlight Ltd. *Spot Series Lasers (Short Pulse Optical Technology)*, 2014.
- [9] Newport Corporation. <http://assets.newport.com/pdfs/g5753.pdf>.
[Online accessed 01-September-2015].
- [10] Linos AG. http://www.linos.com/pages/mediabase/original/fokussierung-aufweitung-von-laserstrahlung_2186.pdf.
[Online accessed 01-September-2015].
- [11] Newport Corporation. <http://physikclub.de/intern/intern/material-und-infos-zu-einzelnen-projekten/laser-und-optik/optik/Fokussieren-Kollimieren.pdf/view>.
[Online accessed 01-September-2015].
- [12] R. Paschotta. https://www.rp-photonics.com/chirped_pulse_amplification.html?s=ak.
[Online accessed 01-September-2015].
- [13] Light Conversion Ltd. *Light Conversion Pharos -Users manual*, 2011.

- [14] Thorlabs Inc. https://www.thorlabs.de/newgrouppage9.cfm?object_group_id=6108.
[Online accessed 01-September-2015].
- [15] IDEX Optics & Photonics. <http://marketplace.idexop.com/store/IdexCustom/PartDetails?pvId=28876&displaySemiCustomTabAsDefault=True&populateBuildYourPartDropdowns=True>.
[Online accessed 01-September-2015].
- [16] J. H. Brannon et al. Excimer laser etching of polyimide. *J. Appl. Phys.*, 58:2036–2043, 1985.
- [17] B. Luk'yanchuk et al. Uv-laser ablation of polyimide: from long to ultra-short laser pulses. *Nuc. Instr. and Meth. in Phys. Res. B*, 122:347–355, 1997.
- [18] M. Himmelbauer et al. Uv-laser-induced surface topology changes in polyimide. *Appl. Phys. A*, 63:337–339, 1996.
- [19] J. H. Brannon and J. R. Lankard. Pulsed co2 laser etching of polyimide. *Appl. Phys. Lett.*, 48:1226–1228, 1986.
- [20] J. Hermani et al. <http://www.diamond-business.de/index.php/artikel-bibliothek/werkzeug-fertigung/laserbearbeitung/item/kurzpuls-laserbearbeitung-von-monokristallinem-cvd-diamant>, 2015.
[Online accessed 02-September-2015].
- [21] Applied Image customer service. <https://www.appliedimage.com/products/test-targets-and-charts-1/usaf-1951-resolution-targets/usaf-1951-standard-resolution-target-t-20>.
[Online accessed 02-September-2015].
- [22] S. M. Kaczmarek et al. Changes in optical properties of yag: Ce single crystals due to codoping and ionising radiation treatment. *Proc. SPIE*, 3724:339–345, 1999.
- [23] Nikon Corporation. <http://www.microscopyu.com/articles/formulas/formulasfielddepth.html>
[Online accessed 07-September-2015].
- [24] W. Demtröder. *Experimentalphysik II Elektrizität und Optik*. Springer Verlag, 2009.
- [25] WTOCD.
<http://www.wtacd.be/en/Techfac/img6B.gif>
<http://www.wtacd.be/en/Techfac/img70.gif>
[Online accessed 08-September-2015].

6 Pictorial Sources

- [1] D. Diercksmeyer, Technical drawing of setup
- [2] B. Reime, Technical drawing of on-axis CCD camera
- [3] <http://www.spektrum.de/lexikon/chemie/polyimid/7304>
[Online accessed 02-September-2015].

```

from PyTango import DeviceProxy, DevFailed
import time

#-----
#Definition der Stepermotoren und Shutter I
devMotorX = DeviceProxy('laserlab/motor/stepper.01')
devMotorY = DeviceProxy('laserlab/motor/stepper.02')
devShutter = DeviceProxy('nano/register/ulab.out01')
#-----

#Anfahren der Startposition mit Wartezeit fuer Motorbewegung
devMotorX.write_attribute("Position",-7500)
time.sleep(0.1)

while str(devMotorX.state()) == "MOVING":
    print "MOVING"
    time.sleep(0.1)

devMotorY.write_attribute("Position",500)
time.sleep(0.1)

while str(devMotorY.state()) == "MOVING":
    print "MOVING Y"
    time.sleep(0.1)

#-----

#Erzeugung von Loechern in einer Reihe

i = -7500
while i < -5000:

    #Abstand der Loecher
    i = i + 20
    print "Variable: %s" % i
    pos = devMotorX.read_attribute("Position").value
    print "Motorposition: %s" % pos
    devMotorX.write_attribute("Position",i)
    while str(devMotorX.state()) == "MOVING":
        print "MOVING"

    #Nachdem Lochposition angefahren oeffnet Shutter
    devShutter.write_attribute("Value", 1)
    status_shutter = devShutter.read_attribute("Value").value
    print "Shutter: %s" % status_shutter
    #Einstellung der Belichtungszeit
    time.sleep(1)
    devShutter.write_attribute("Value", 0)
    status_shutter = devShutter.read_attribute("Value").value
    print "Shutter: %s" % status_shutter
    time.sleep(0.2)

#-----

```

```

from PyTango import DeviceProxy, DevFailed
import time
import math
import numpy

#-----|-----

#Definition der Stepermotoren und Shutter
devMotorX = DeviceProxy('laserlab/motor/stepper.01')

devMotorY = DeviceProxy('laserlab/motor/stepper.02')

devShutter = DeviceProxy('nano/register/ulab.out01')

#-----

#Startwerte x und y Position
x_start = 0
y_start = 0

#Startwerte der Spiral- (b) und Kreiswinkel (a)
a = 0
b = 0

#Startwert fuer variablen Radius der Spirale
radius_var = 0

#Boolesche Variable fuer spaeteres Hochzaehlen von a
v = 0

#Zu waehlender Kreisradius
radius = 500

#-----

#Anfahren der Startposition
devMotorX.write_attribute("Position",x_start)
time.sleep(0.1)

while str(devMotorX.state()) == "MOVING":
    print "MOVING X"
    time.sleep(0.1)

devMotorY.write_attribute("Position",y_start)
time.sleep(0.1)

while str(devMotorY.state()) == "MOVING":

#-----

#Spirale in Kreis mit gewaehltem Radius
while b < 4*numpy.pi :

    #Radiuszunahme
    radius_var = radius_var + 5

    #x-Position
    x = radius_var * numpy.cos(b)
    print "MotorpositionX: %s" % x
    devMotorX.write_attribute("Position",x)
    time.sleep(0.1)
    while str(devMotorX.state()) == "MOVING":
        print "MOVING"
        time.sleep(0.05)

    #y-Position
    y = radius_var * numpy.sin(b)
    print "MotorpositionY: %s" % y
    devMotorY.write_attribute("Position",y)
    time.sleep(0.1)
    while str(devMotorY.state()) == "MOVING":
        print "MOVING"
        time.sleep(0.05)

```

```

#Abbruch der Spirale, wenn der Radius des Kreises erreicht ist
if numpy.sqrt(x*x + y*y) >= radius:

    #Dann wird der Kreis mit dem gewaehlten Radius berechnet
    while a < 4*numpy.pi:

        #Einfuehrung einer Booleschen Variablen v.
        #Zunaechst wird b einmalig an a uebergeben.
        #Nach dem Umschalten wird der Kreiswinkel a hochgezaehlt.
        if v == 0:
            a = b
            v = 1
        a = a + numpy.pi/500

        #x-Position
        x = radius * numpy.cos(a)
        print "MotorpositionX: %s" % x
        devMotorX.write_attribute("Position",x)
        time.sleep(0.05)
        while str(devMotorX.state()) == "MOVING":
            print "MOVING"

        #y-Position
        y = radius * numpy.sin(a)
        print "MotorpositionY: %s" % y
        devMotorY.write_attribute("Position",y)
        time.sleep(0.05)
        while str(devMotorY.state()) == "MOVING":
            print "MOVING"
            time.sleep(0.05)
        b = b + numpy.pi/500

    #Abbruch der ersten while-Schleife
    break

#Ansonsten wird der Spiralwinkel b hochgezaehlt
else:
    b = b + numpy.pi/100

#-----

```